Resonance Raman Characterization of the Mononuclear Iron Active-Site Vibrations and Putative Electron Transport Pathways in *Pyrococcus furiosus* Superoxide Reductase†

Michael D. Clay,‡ Francis E. Jenney, Jr.,§ Hak Joon Noh,§ Peter L. Hagedoorn,‡,|| Michael W. W. Adams,§ and Michael K. Johnson‡,*

Departments of Chemistry and Biochemistry & Molecular Biology, and Center for Metalloenzyme Studies, University of Georgia, Athens Georgia 30602

Received March 18, 2002; Revised Manuscript Received June 7, 2002

ABSTRACT: The resonance Raman spectrum of oxidized wild-type *P. furiosus* SOR at pH 7.5 and 10.5 has been investigated using excitation wavelengths between 406 and 676 nm, and vibrational modes have been assigned on the basis of isotope shifts resulting from global replacements of ^{32}S with ^{34}S, ^{14}N with ^{15}N, ^{56}Fe with ^{54}Fe, and exchange into a $H_2{}^{18}O$ buffer. The results are interpreted in terms of the crystallographically defined active-site structure involving a six-coordinate mononuclear Fe center with four equatorial histidine ligands and axial cysteine and monodentate glutamate ligands (Yeh, A. P., Hu, Y., Jenney, F. E., Adams, M. W. W., and Rees, D. C. (2000) *Biochemistry 39*, 2499−2508). Excitation into the intense (Cys)S(p_π)-to-Fe(d_π) CT transition centered at 660 nm results in strong enhancement of modes at 298 cm^{-1} and 323 cm^{-1} that are assigned to extensively mixed cysteine S−C_β−C_α bending and Fe−S(Cys) stretching modes, respectively. All other higher-energy vibrational modes are readily assigned to overtone or combination bands or to fundamentals corresponding to internal modes of the ligated cysteine. Weak enhancement of Fe−N(His) stretching modes is observed in the 200−250 cm^{-1} region. The enhancement of internal cysteine modes and Fe−N(His) stretching modes are a consequence of a near-planar Fe−S−C_β−C_α−N unit for the coordinated cysteine and significant (His)N(p_π)−Fe(d_{xy})−(Cys)S-(p_π) orbital overlap, respectively, and have close parallels to type 1 copper proteins. By analogy with type 1 copper proteins, putative superexchange electron-transfer pathways to the mononuclear Fe active site are identified involving either the tyrosine and cysteine residues or the solvent-exposed δN histidine residue in a Y−C−X−X−H arrangement. Studies of wild-type at pH 10.5 and the E14A variant indicate that the resonance Raman spectrum is remarkably insensitive to changes in the ligand trans to cysteine and hence are inconclusive concerning the origin of the alkaline transition and the nature of sixth Fe ligand in the E14A variant.

Evidence has recently accumulated for a novel oxidative stress pathway in anaerobes involving superoxide reduction rather than dismutation (*1*, *2*). The key enzyme in this pathway, superoxide reductase (SOR),[1] catalyzes the reduction of superoxide to hydrogen peroxide and appears to use rubredoxin as the immediate electron donor (*1*, *3*). Distinct forms of SOR containing 1Fe and 2Fe atoms per monomer have been characterized and are commonly referred to by the trivial names neelaredoxin (*4*) and desulfoferrodoxin (*5*), respectively. Both contain a common mononuclear non-heme Fe site, but the 2Fe−SORs contain an additional desulforedoxin domain containing a rubredoxin-type Fe($SCys)_4$ center. Crystallographic and spectroscopic studies of the 2Fe−SOR from *Desulfovibrio desulfuricans* (*6*, *7*) and the 1Fe−SOR from *Pyrococcus furiosus* (*8*, *9*) have revealed an SOR active-site comprising a mononuclear Fe with four equatorial histidyl ligands (one δN and three ϵN) and one axial cysteinyl ligand. A monodentate glutamate (E14) completes octahedral coordination in oxidized *P. furiosus* SOR but is removed on reduction, creating a binding site trans to the cysteinate for substrate binding and activation (*8*, *9*).

The ground- and excited-state electronic properties of the ferric and ferrous sites in *P. furiosus* SOR have recently been extensively characterized using the combination of EPR, absorption, CD, and variable-field, variable-temperature magnetic circular dichroism (VHVT MCD) spectroscopies (*9*). This has led to detailed assignments of ligand-field and ligand-to-metal charge transfer (CT) transitions and assessment of the important role of (Cys)S(p_π)−Fe(d_π) interactions for optimizing the active site for reductive binding of

† This work was supported by a grant from the National Institutes of Health (GM60326 to M.W.W.A. and M.K.J.) and a National Science Foundation Research Training Group Award to the Center for Metalloenzyme Studies (DBI9413236).

* Corresponding author. Tel.: 706-542-9378. Fax: 706-542-2353. E-mail: johnson@chem.uga.edu.

‡ Department of Chemistry and Center for Metalloenzyme Studies.

§ Department of Biochemistry & Molecular Biology and Center for Metalloenzyme Studies.

|| Present address: Department of Biotechnology, Delft University of Technology, The Netherlands.

[1] Abbreviations: SOR, superoxide reductase; VHVT MCD, variable-field, variable-temperature magnetic circular dichroism; CT, charge transfer.

10.1021/bi025833b CCC: $22.00
Published on Web 07/12/2002

superoxide and dissociation of the peroxide product (*9*, *10*). In addition, the results indicate the potential of resonance Raman, using excitation into S-to-Fe CT transitions, for monitoring Fe−S(Cys) vibrational modes and the changes in the active site during catalytic turnover. Although resonance Raman of the 2Fe−SOR from *D. desulfuricans* provided the original evidence for cysteinate coordination of the oxidized SOR active site (*6*), detailed vibrational assignments were not attempted due to the complications associated with the presence of an additional cysteinyl-ligated Fe site. In this work, we report assignment of the resonance Raman spectrum of oxidized wild-type *P. furiosus* SOR at pH 7.5 and 10.5, based on isotope shifts resulting from global replacements of ^{32}S with ^{34}S, ^{14}N with ^{15}N, ^{56}Fe with ^{54}Fe, exchange into a $H_2{}^{18}O$ buffer, and parallel resonance Raman studies of the oxidized E14A variant. The results reveal extensive coupling between the Fe−S stretching mode and the internal vibrational modes of cysteine. On the basis of the evidence for substantial $S(p_\pi)$−$Fe(d_\pi)$ interactions (*9*, *10*) and the close analogy with type 1 (blue) copper proteins, the resonance Raman results suggest superexchange pathways for mediating electron transfer from rubredoxin to the mononuclear Fe active site.

MATERIALS AND METHODS

Sample Preparation. The gene encoding wild-type *P. furiosus* SOR was expressed in *Escherichia coli*, and the recombinant protein was purified to homogeneity according to the published procedure (*9*). The E14A variant of *P. furiosus* SOR was generated using a standard mutagenesis kit (QuikChange Site-Directed Mutagenesis Kit, Stratagene, La Jolla, CA), and the DNA sequence was confirmed. The recombinant E14A SOR was purified in the same manner as that for the wild-type protein. Samples of wild-type *P. furiosus* SOR globally labeled with ^{15}N and ^{34}S SOR were obtained in the same way, except that *E. coli* was grown in 2.8 L flasks (6 × 1 L), shaking at 250 rpm. For the ^{15}N-labeled sample, $^{15}NH_4Cl$ (98% enriched; Cambridge Isotopes) was substituted for NH_4Cl and $FeCl_3$ substituted for $Fe(NH_4)_2(SO_4)_2$ in the M9 salts. For the ^{34}S-labeled sample, $MgCl_2$ was substituted for $MgSO_4$, and the sole source of sulfur was 2mM $^{34}SO_4{}^{2-}$ prepared in a 100 mM potassium phosphate buffer. $^{34}SO_4{}^{2-}$ was prepared by heating elemental ^{34}S (99.8% enriched; Trace isotopes) to 85 °C in aqua regia. For the ^{54}Fe-labeled sample, ^{54}Fe ferric citrate (95% enrichment) was substituted for $FeCl_3$ in the M9 salts. The ^{54}Fe ferric citrate solution was prepared from ^{54}Fe metal by dissolving in aqua regia, adding stoichiometric sodium citrate, and neutralizing with 10% ammonium hydroxide. Prior to use for spectroscopic studies, samples were oxidized with excess hexachloroiridate, and the excess oxidant was removed by Amicon ultrafiltration. Samples at pH 7.5 were in 50 mM HEPES buffer. Samples at pH 10.5 were prepared by Amicon buffer exchange into a 50 mM CAPS, pH 10.5 buffer, and samples in $H_2{}^{18}O$ (95−98% enrichment) were prepared by Amicon buffer exchange using the equivalent $H_2{}^{18}O$ buffer. In each case buffer exchange involved three 10-fold dilution and concentration cycles.

Spectroscopic Methods. Resonance Raman spectra were recorded using an Instruments SA Ramanor U1000 spectrometer fitted with a cooled RCA-31034 photomultiplier tube with 90° scattering geometry. Spectra were recorded digitally using photon counting electronics, and improvements in signal-to-noise were achieved by signal averaging multiple scans. Absolute band positions were calibrated using the excitation frequency and CCl_4 and are accurate to ±1 cm^{-1}. Lines from a Coherent Sabre 100 10-W Argon Ion Laser or Coherent Innova 200-K2 Krypton Ion Laser were used for excitation, and plasma lines were removed using a Pellin Broca prism premonochromator. Scattering was collected from the surface of a frozen 10-μL droplet of sample using a custom-designed anaerobic sample cell (*11*), attached to the coldfinger of an Air Products Displex Model CSA-202E closed cycle refrigerator. This arrangement enables samples to be cooled to 17 K, which facilitates improved spectral resolution and prevents laser-induced sample degradation. For excitation profiles, 0.5 M sodium sulfate was added to the sample in order to provide an internal standard for the SOR vibrational modes. For assessment of isotope shifts, both the natural abundance and isotopically enriched samples were placed on the sample probe, and frequency calibration was checked before and after measurements to ensure relative accuracy of band positions to at least ±0.1 cm^{-1}. Isotope shifts ($\Delta\nu$) were assessed to an accuracy of ±1 cm^{-1} for weak bands based on spectral overlays and to an accuracy of ±0.2 cm^{-1} for more intense bands based on the natural abundance minus isotopically labeled difference spectrum using the relationship $\Delta\nu = I_D\Gamma/2.6I$, where I_D is the peak-to-trough intensity of the difference spectrum, I is the maximum peak intensity, and Γ is the full width at half-height (*12*).

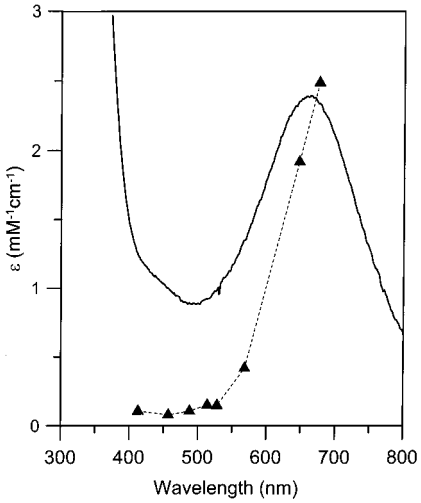

FIGURE 1: Visible absorption spectrum and resonance Raman excitation profile for the 323 cm^{-1} vibrational mode of wild-type *P. furiosus* SOR. The sample and Raman measurement conditions are the same as those described in Figure 2, except for the addition of 500 mM sodium sulfate, which served as an internal standard for the excitation profile. The excitation profile (▲) is in arbitrary units and corresponds to the ratio of the intensity of the 323 cm^{-1} band of SOR to the 990 cm^{-1} symmetric stretch of the sulfate anion at different excitation wavelengths.

RESULTS

Fe−S(Cys) Vibrational Modes. The visible absorption spectrum of oxidized wild-type *P. furiosus* SOR is dominated by an intense $(Cys)S(p_\pi)$-to-$Fe(d_\pi)$ CT transition centered at 660 nm (*9*) (see Figure 1). In accord with this assignment, strong enhancement of vibrational modes associated with the Fe−S(Cys) unit are observed in the resonance Raman

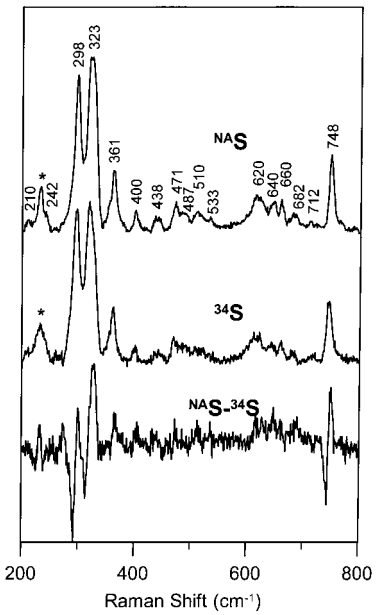

FIGURE 2: Resonance Raman spectra of natural abundance (NA) and ^{34}S globally labeled wild-type *P. furiosus* SOR. Upper spectrum: natural abundance. Middle spectrum: globally enriched with ^{34}S. Lower spectrum: Natural abundance minus ^{34}S globally enriched difference spectrum. Spectra recorded using 647 nm excitation with samples as frozen droplets maintained at 17 K. Samples were ~5 mM in SOR and were in 50 mM HEPES pH 7.5 buffer. Spectra were recorded using 6 cm^{-1} resolution by photon counting for 1 s every 1 cm^{-1} and are the sum of 30−50 scans. The asterisks indicate lattice modes of ice.

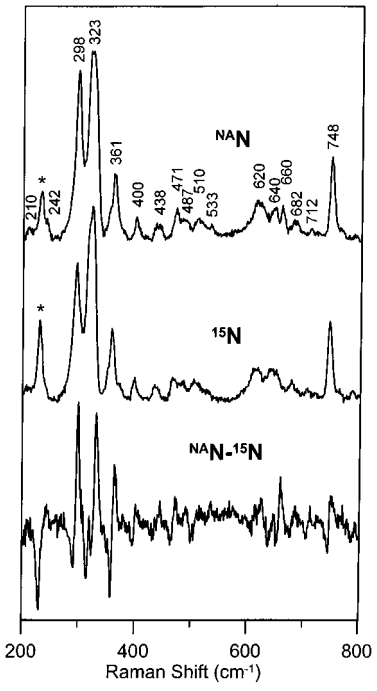

FIGURE 3: Resonance Raman spectra of natural abundance (NA) and ^{15}N globally labeled wild-type *P. furiosus* SOR. Upper spectrum: natural abundance. Middle spectrum: globally enriched with ^{15}N. Lower spectrum: Natural abundance minus ^{15}N globally enriched difference spectrum. The sample and measurement conditions are the same as those described in Figure 2, and asterisks indicate the lattice modes of ice.

spectrum using 647 nm excitation (see Figures 2−4 and Table 1). The excitation profile for the most intense band at 323 cm^{-1}, which contains a major contribution from Fe−S(Cys) stretching (see below), reveals maximal enhancement to the low-energy side of the 660 nm absorption band (see Figure 1). Analogous excitation profiles, albeit with lower cross-sections, were observed for all of the Raman bands in 250−800 cm^{-1} region (data not shown), indicating that all are enhanced via kinematic coupling with the Fe−S(Cys) stretching mode or an excited-state *A*-term mechanism involving the extended Fe−cysteinate chromophore. The vibrational assignments in this region, based on globally labeled ^{34}S, ^{15}N, and ^{54}Fe isotope shift data (Figures 2, 3, and 4 respectively), are presented in Table 1 and discussed below.

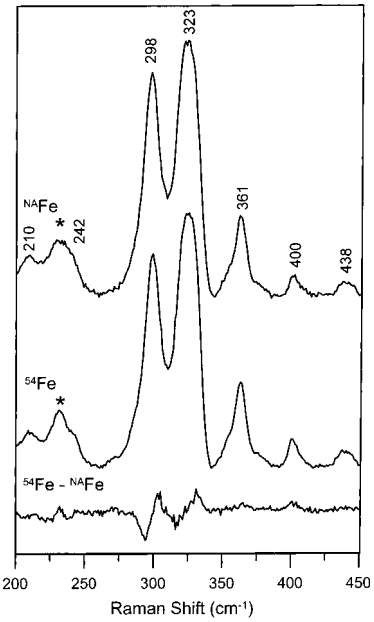

FIGURE 4: Resonance Raman spectra of natural abundance (NA) and ^{54}Fe globally labeled wild-type *P. furiosus* SOR. Upper spectrum: natural abundance. Middle spectrum: globally enriched with ^{54}Fe. Lower spectrum: ^{54}Fe minus natural abundance difference spectrum. The sample and measurement conditions are the same as those described in Figure 2, and the asterisk indicates a lattice mode of ice.

The low-frequency region is dominated by three bands centered at 298, 323, and 748 cm^{-1}, which are identified as fundamental vibrations involving movement of cysteinyl S via ^{34}S downshifts in excess of 2 cm^{-1}. The 298 and 748 cm^{-1} bands are assigned to $S-C_\beta-C_\alpha$ bending and $S-C_\beta$ stretching modes, respectively, on the basis of the extensive vibrational studies and normal modes calculations that are available for Fe−S proteins (*13*−*16*) and type 1 copper proteins (*15*−*19*). The most intense band at 323 cm^{-1} has the largest ^{34}S downshift and is, therefore, assigned primarily to Fe−S(Cys) stretching. However, the observed 3.3 cm^{-1} ^{34}S downshift and 1.1 cm^{-1} ^{54}Fe-upshift (see Table 1) are just over half of the 6 cm^{-1} ^{34}S downshift and 2 cm^{-1} ^{54}Fe upshift that are predicted based on a simple Fe−S diatomic oscillator approximation, suggesting significant mixing with internal vibrational modes of the coordinated cysteine residue.

Evidence for mixing of the Fe−S(Cys) stretching mode with cysteine deformations comes from the enhancement of at least six modes, at 361, 400, 438, 471, 487, and 510 cm^{-1}, in the region associated with deformation modes of the coordinated cysteine and the peptide backbone of adjacent residues in type 1 copper proteins (*17*−*21*). In support of

Table 1: Assignment of the Resonance Raman Spectrum of Oxidized Wild-Type *P. furiosus* SOR

frequency, cm^{-1}	^{34}S shift,[a] cm^{-1}	^{15}N shift,[a] cm^{-1}	^{54}Fe shift,[a] cm^{-1}	assignment[b]
210	0	−2	0	(Fe−N(His))
234	0	−1	nd	ν(Fe−N(His))[c]
242	0	−2	+1	ν(Fe−N(His))
298	−2.2	−2.2	+1.1	$\delta(S-C_\beta-C_\alpha) + \nu(Fe-S)$
323	−3.3	−1.5	+1.1	$\nu(Fe-S) + \delta(S-C_\beta-C_\alpha)$
361	−1.0	−4.0	0	$\delta(C_\beta-C_\alpha-C(O))$
400	−1	−3	0	$+ \delta(C_\beta-C_\alpha-N)$
438	0	−2	0	$+ \delta(C(O)-C_\alpha-N)$
471	−1	−5	0	$+ \delta(C_\alpha-N-C(O))$
487	0	−3	0	$+ \delta(S-C_\beta-C_\alpha)$
510	0	−5	0	$+\nu$(Fe−S)
533	−3	−4	+1	combination (210 + 323)
620	−5	−4	+2	combination (298 + 323)
640	−5	−3	+2	overtone (2 × 323)
660	0	−7	0	$\nu(C_\alpha-N)$
682	−3	−5	+1	combination (323 + 361)
712	−1	−6	0	overtone (2 × 361)
748	−2.7	−1.1	0	$\nu(S-C_\beta)$
1003	0	nd	nd	phenylalanine
1110	0	nd	nd	$\nu(C_\beta-C_\alpha)$
1227	0	nd	nd	$C_\beta H_2$ twisting
1302	0	nd	nd	amide III
1431	0	nd	nd	$C_\beta H_2$ scissoring
1553	0	nd	nd	amide II
1662	0	nd	nd	amide I

[a] Isotope shifts given to two significant figures have an estimated uncertainty of ±0.2 cm^{-1}, and those given to one significant figure have an estimated uncertainty of ±1 cm^{-1}; nd, not-determined. [b] Unless otherwise indicated, all assignments correspond to vibrational modes of Cys111 and indicate the major contributing modes. [c] Obscured by lattice mode of ice in $H_2{}^{16}O$ buffer.

this assignment, the bands at 361, 400, and 471 cm^{-1} in *P. furiosus* SOR each exhibit ^{34}S downshifts of approximately 1 cm^{-1} (see Figure 2 and Table 1), indicating significant kinematic coupling. Moreover, each of the bands in this region exhibits a ^{15}N downshift in the range 2−5 cm^{-1}, indicating contributions from the $C_\beta-C_\alpha-N$, $C(O)-C_\alpha-N$ and $C_\alpha-N-C(O)$ deformations of the coordinating cysteine and the peptide backbone of adjacent residues. ^{15}N downshifts of similar magnitude have been observed for the equivalent bands in type 1 copper proteins (*18*, *19*, *21*, *22*), and in the case of type 1 copper proteins, selective ^{15}N labeling of the imidazoles of the coordinating histidines has shown these modes are primarily associated with deformation modes of the coordinated cysteine and the peptide backbone of adjacent residues, rather than of coordinating histidine residues (*18*).

Since kinematic coupling is critically dependent on the energy separation of the uncoupled modes, the most extensive mixing is expected to occur between the Fe−S(Cys) stretching and cysteine $S-C_\beta-C_\alpha$ bending modes, which are assigned to the intense bands at 323 and 298 cm^{-1}, respectively. This is confirmed by the ^{54}Fe isotope shifts, 1.1 cm^{-1} upshifts for both the 323 and 298 cm^{-1} bands (see Figure 4 and Table 1), indicating that these vibrational modes are extensively mixed. In addition, evidence for mixing of the 361 and 298 cm^{-1} modes with the 323 cm^{-1} mode in SOR comes from the change in the relative intensity of the 323 and 298 cm^{-1} modes in the ^{15}N globally labeled spectrum (see Figure 3). This change in relative intensity is reproducible with different samples and is responsible for the unsymmetrical derivatives associated with the 298 and 323 cm^{-1} bands in the $^{NA}N-^{15}N$ difference spectrum (Figure 3). The change in relative intensity is readily rationalized in terms of enhanced mixing between the 323 and 361 cm^{-1} modes in the ^{15}N globally labeled spectrum, as a result of the large ^{15}N downshift in the 361 cm^{-1} band (4 cm^{-1}), coupled with a concomitant decrease in the mixing between the 323 and 298 cm^{-1} modes.

Weak bands in the 520−750 cm^{-1} region are readily assigned to overtones and combination bands on the basis of additivity of natural abundance frequencies and ^{34}S, ^{15}N, and ^{54}Fe isotope shifts (see Figures 2−4 and Table 1). The only exception is the band at 660 cm^{-1}, which has a negligible ^{34}S downshift and a large ^{15}N downshift (7 cm^{-1}). The absence of a ^{34}S downshift rules out assignment to a 298 + 361 cm^{-1} combination band. Hence, it is assigned to a fundamental with significant cysteine $C_\alpha-N$ stretching character, on the basis of normal mode calculations for L-cysteine (*23*). In accord with this assignment, numerous additional modes associated with internal modes of the ligated cysteine are observed in the high-frequency region (see Figure 5). With the exception of the weak band at 1003 cm^{-1}, which is assigned to the most intense mode of nonresonantly enhanced phenylalanine (there are four Phe residues in *P. furiosus* SOR), the bands at 1100, 1227, 1302, 1431, 1553, and 1662 cm^{-1} are all enhanced in resonance with the 660 nm absorption band. On the basis of the isotope shifts observed in cysteine−$C_\beta D_2$-labeled type 1 copper proteins (*19*), normal mode calculations for L-cysteine (*23*), and the frequency ranges observed for polypeptide amide I, II, and III modes in Raman spectra (*24*), these modes are readily assigned to the $C_\beta-C_\alpha$ stretching, $C_\beta H_2$ twisting, amide III, $C_\beta H_2$ scissoring, amide II ,and amide I vibrations, respectively, primarily involving the ligated cysteine. All of these modes exhibit negligible ^{34}S isotope shifts indicating enhancement via an excited-state *A*-term mechanism, i.e., distortion of internal cysteine bonds in the electronic excited-state associated with the $(Cys)S(p_\pi)$-to-$Fe(d_\pi)$ CT transition.

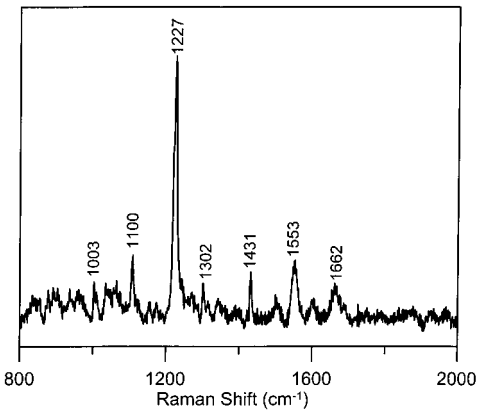

FIGURE 5: Resonance Raman spectrum of wild-type *P. furiosus* SOR in the high-frequency region, 800−2000 cm^{-1}. The sample and measurement conditions are the same as those described in Figure 2.

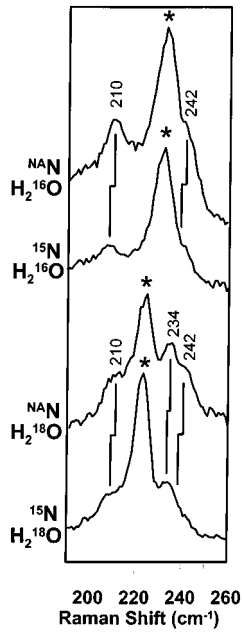

FIGURE 6: Resonance Raman spectra of natural abundance (NA) and ^{15}N globally labeled wild-type *P. furiosus* SOR in the Fe−N(His) stretching region, 190−260 cm^{-1}. The two upper spectra were recorded in $H_2{}^{16}O$ 50 mM HEPES pH 7.5 buffer, and the two lower spectra were recorded after exchange into $H_2{}^{18}O$ 50 mM HEPES pH 7.5 buffer. All other sample and measurement conditions are the same as those described in Figure 2, except that each spectrum is the sum of at least 100 scans. Bands arising from lattice modes of frozen $H_2{}^{16}O$ or $H_2{}^{18}O$ are indicated by asterisks.

Fe−N(His) Stretching Modes. Weakly enhanced modes that are candidates for Fe−N(His) stretching modes are observed in the 190−250 cm^{-1} region (see Figure 6). Exchanging the buffer from $H_2{}^{16}O$ to $H_2{}^{18}O$, to shift the lattice modes of ice from 231 to 222 cm^{-1}, facilitates observation of a band centered at 210 cm^{-1} and another at 234 cm^{-1} with a pronounced shoulder at 242 cm^{-1} that each exhibit 1−2 cm^{-1} isotope shift in ^{15}N globally labeled samples and negligible isotope shifts in ^{34}S globally labeled samples (see Figure 6 and Table 1). The ^{15}N isotope shifts are in the range expected for Fe−N(His) stretching modes, which is predicted to be ~1.5 cm^{-1} on the basis of a diatomic Fe−imidazole oscillator. These modes are therefore good candidates for the symmetric and asymmetric stretching modes, respectively, of one or both pairs of trans histidine residues which have Fe−N distances in the range 2.1−2.2 Å (*8*, *9*). Fe−N(His) stretching modes are not expected to be enhanced by kinematic coupling with Fe−S(Cys) stretching, since the Fe−S bond is perpendicular to the FeN_4 plane, and this is in accord with the lack of measurable ^{34}S isotope shifts. However, Fe−N(His) stretching modes could be weakly enhanced via an *A*-term mechanism, i.e., distortion of the Fe−N(His) bonds in the electronic excited-state associated with the (Cys)S(p_π)-to-Fe(d_π) CT transition. UV resonance Raman studies are planned, using excitation into the intense CT band centered at 330 nm, to assess the validity of these assignments. The 330 nm absorption band has been shown to have contributions from His-to-Fe^{3+} CT transitions based on VHVT MCD studies (*9*).

Wild-Type pH 10.5 and E14A Variant. Optical pH titrations of oxidized *P. furiosus* SOR revealed an alkaline transition with a $pK_a = 9.6$ (*9*). The alkaline transition is marked by a shift in the (Cys)S(p_π)-to-Fe(d_π) CT transition from 660 nm to 590 nm (*9*). Moreover, the resultant UV−visible absorption spectrum for wild-type SOR at pH 10.5 is almost indistinguishable from that of the E14A variant at pH 7.5 (see Supporting Information, Figure S1), suggesting that the change in Fe ligation induced by mutating the glutamate ligand is the same as that induced in wild-type at alkaline pH. In an attempt to investigate the change in ligation, resonance Raman spectra of wild-type SOR at pH 10.5 and the E14A variant at pH 7.5 were recorded in the region 200−800 cm^{-1} using 647 nm excitation, and compared with equivalent spectra obtained for wild-type at pH 7.5 (see Figure 7). Remarkably the spectra of all three samples are essentially the same within experimental error, both in terms of the relative intensities and the frequencies of individual modes. Moreover, the same result was observed using 568 nm excitation which is close to the maxima of the (Cys)S(p_π)-to-Fe(d_π) CT absorption in the wild-type pH 10.5 and E14A samples (see Supporting Information, Figure S2). The only minor difference is that the intensities of the internal cysteine modes were significantly increased relative to those of the Fe−S(Cys) stretching modes in the E14A variant compared to the wild-type samples using 568 nm excitation. The resonance Raman results clearly demonstrate that the marked changes in the energy of the (Cys)S(p_π)-to-Fe(d_π) CT transition that are associated with the alkaline transition and the E14A mutation do not result from changes in the cysteinyl or histidyl Fe ligation.

Unfortunately, the resonance Raman spectra of wild-type samples at pH 7.5 and 10.5 and of the E14A variant provide no direct evidence in the form of an Fe−ligand stretching mode for the existence of a ligand trans to the cysteinyl S. Such a mode might be expected to be weakly enhanced via excitation into (Cys)S(p_π)-to-Fe(d_π) CT transition via kinematic coupling with the Fe−S(Cys) stretching mode. Since no bands are lost or undergo a significant decrease in intensity in the wild-type pH 10.5 or E14A spectra, we conclude that an Fe−O(Glu) stretching mode is either not present or not enhanced. The possibility that the sixth ligand in the three derivatives investigated is derived from an exchangeable water molecule (i.e., H_2O or OH^-) was investigated by recording resonance Raman spectra of the wild-type pH 7.5, wild-type pH 10.5, and E14A variant samples after exchange into equivalent $H_2{}^{18}O$ buffer (see Supporting Information Figures S3, S4, and S5, respectively).

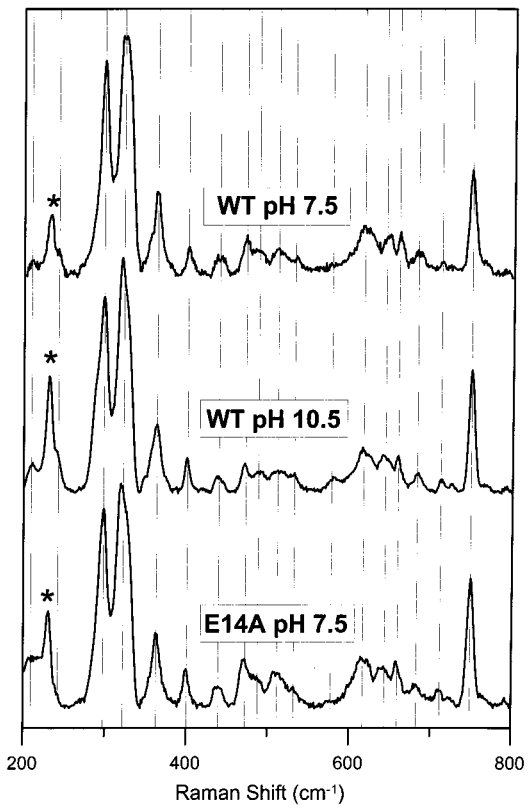

FIGURE 7: Comparison of the resonance Raman spectra of wild-type *P. furiosus* SOR at pH 7.5 and 10.5 with the E14A variant at pH 7.5. Upper spectrum: wild-type at pH 7.5. Middle spectrum: wild-type at pH 10.5. Lower spectrum: E14A variant at pH 7.5. The sample and measurement conditions are the same as those described in Figure 2, except that pH 10.5 sample was in 50 mM CAPS buffer. The asterisk indicates a lattice mode of ice.

Other than the expected isotope shift in the lattice mode of ice from 231 to 222 cm^{-1}, none of the bands in any of these derivatives was perturbed by exchange into $H_2{}^{18}O$ buffer. Once again, this result should not be interpreted in terms of the absence of a water derived ligand, merely that such a ligand, if present, is either not exchangeable or has an Fe−O stretching mode that is not significantly resonantly enhanced. Since a weak mode at 580 cm^{-1} was observed with 647 nm excitation in the wild-type pH 10.5 and E14A variant spectra, but not in the wild-type pH 7.5 spectra (Figure 7), we explored the possibility that this mode may originate from an Fe−N stretching mode of a coordinated lysine ligand. Several observations argue against this interpretation. First, a weak mode at 580 cm^{-1} is observed in wild-type SOR at pH 7.5 with 568 nm excitation (see Supporting Information Figure S2). Second, the 580 cm^{-1} band in the wild-type pH 10.5 sample undergoes a 4 cm^{-1} downshift in samples globally labeled with ^{15}N (see Supporting Information Figure S6). Hence, the observed isotope shift is more in line with an internal cysteine mode than an Fe−N(Lys) mode which would be expected to have a 15 cm^{-1} ^{15}N downshift base on a simple diatomic oscillator approximation.

DISCUSSION

Resonance Raman studies of *P. furiosus* SOR using excitation into the intense (Cys)S(p_π)-to-Fe(d_π) CT transition have revealed extensive enhancement of vibrational modes associated with the ligated cysteine residue and weak enhancement of Fe−N(His) stretching modes. While the most intense band is attributed primarily to Fe−S(Cys) stretching, numerous fundamentals of the ligated cysteine, including δ(S−C_β−C_α), δ(C_β−C_α−C(O)), δ(C_β−C_α−N), δ-(C(O)−C_α−N), δ(C_α−N−C(O)), ν(C_α−N), ν(S−C_β), ν(C_β−C_α), $C_\beta H_2$ twisting, $C_\beta H_2$ scissoring, and amide I, II, and III modes, are also enhanced. Isotope shift data using samples globally labeled with ^{34}S and ^{54}Fe indicate that the enhancements arise from both kinematic coupling with the Fe−S(Cys) stretching mode and an excited-state *A*-term mechanism involving the extended Fe-cysteinate chromophore and one or more of the Fe−N(His) ligands.

By analogy with type 1 copper proteins, kinematic coupling between Fe−S stretching and internal cysteine modes in SOR is likely to be mediated by the HC_α−$C_\beta H$ torsional mode (*20*) and is expected to be maximal for an Fe−S−C_β−C_α dihedral angle close to 180° and a planar Fe−S−C_β−C_α−N unit (*15*, *18*, *25*). This prediction is borne out by the crystal structure of *P. furiosus* SOR, which indicates Fe−S−C_β−C_α and S−C_β−C_α−N dihedral angles close to 155° and 170° and hence a near-planar Fe−S−C_β−C_α−N unit (*8*). Only the modes that are close in energy to the Fe−S(Cys) stretching mode (±150 cm^{-1}) appear to be enhanced via kinematic coupling, as evidence by significant ^{34}S and/or ^{54}Fe shifts.

Cysteine internal modes and Fe−N(His) stretching modes that exhibit negligible ^{34}S isotope shifts appear to be enhanced by an excited-state *A*-term mechanism, whereby the vibrations mimic the distortion in the electronic excited state of the (Cys)S(p_π)-to-Fe(d_π) CT transition. Previous studies of the ground- and excited-state electronic structure of *P. furiosus* SOR have emphasized the importance of the S(p_π)−Fe(d_π) interaction in facilitating substrate reduction and promoting product release in SOR (*9*, *10*). Hence, the modes enhanced in the resonance Raman spectrum via an *A*-term mechanism may be directly relevant to the electron-transfer pathway (*19*, *26*, *27*), since the charge-transfer excited state with a hole on the cysteinyl S can correspond to a virtual state in a superexchange model of the electron-transfer process (*28*).

The parallels between type 1 copper proteins and SORs with respect to electron transport pathways are particularly striking. For example, in plastocyanin, an archetypical type 1 copper protein, the tyrosine residue and cysteine ligands that mediate electron transport from cytochrome b_6f to Cu (*29*, *30*) and the δN-histidine ligand that mediates electron transfer from Cu to photosystem I (*31*, *32*), are in Y−C−X−P−H arrangement (*19*). The tyrosine side chain is solvent exposed, and the superexchange pathway for electron entry is maximized by extending the coplanar arrangement of the Cu−S−C_β−C_α−N unit to the adjacent tyrosine residue, thereby facilitating long-range electronic coupling (*19*). An analogous Y−C−X−X−H arrangement of the cysteine and sole δN-histidine ligands to the Fe center is conserved in all 2Fe−SORs and the majority of the 1Fe−SORs (*33*). The only exceptions are the 1Fe−SORs from *Treponema pallidum* and *Desulfovibrio gigas* (F in place of Y) and from *Methanococcus jannaschii* (R in place of Y) (*33*). The crystal structures of the 2Fe−SOR from *D. desulfuricans* (*7*) and the 1Fe−SOR from *P. furiosus* (*8*) show that the coplanar arrangement of the Fe−S−C_β−C_α−N unit extends to the adjacent tyrosine residue, but with the tyrosine side chain

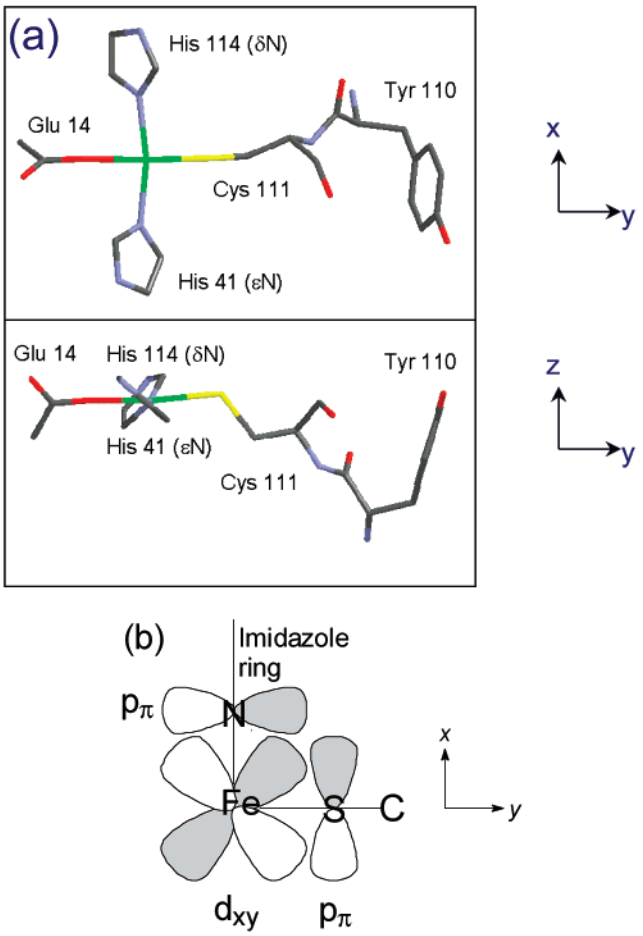

FIGURE 8: (a) Top and side view of the *P. furiosus* SOR active site showing the near-planar arrangement of the Fe−S−C_β−C_α−N unit and the orientation of the histidine imidazoles with respect to the FeN_2S plane defined by His114(δN) and His41(ϵN). The coordinates were taken from the Protein Data Base entry for oxidized *P. furiosus* SOR (subunit A) (*8*), and the axes correspond to the zero-field splitting axis system as determined by EPR and VHVT MCD studies (*9*). The imidazole rings of the two other equatorial histidines, His16(ϵN) and His47(ϵN), have been omitted for clarity. (b) Schematic depiction of optimal orbital overlap between the Fe(d_{xy}) and CysS(p_π) and HisN(p_π) orbitals, i.e., with the plane of the imidazole ring 90° to the FeN_2S plane. In *P. furiosus* SOR, the imidazole rings of His41(ϵN) and His114(δN) are ~50° to the FeN_2S plane.

perpendicular rather than coplanar as in type 1 copper proteins (see Figure 8).

An electron-transfer pathway via the tyrosine and cysteine residues is an attractive possibility in 2Fe−SORs, since the tyrosine side chain lies on the direct path between the rubredoxin-type $Fe(SCys)_4$ center and the mononuclear Fe active site. Previously, the viability of electron transfer from the $Fe(SCys)_4$ center in 2Fe−SORs has been questioned since the Fe−Fe distance, ~22 Å (*34*), is significantly longer than the range commonly associated with electron tunneling between metal centers in metalloproteins (≤14 Å) (*35*). Characterization of a superexchange pathway contributes a high electronic coupling matrix element that may facilitate tunneling over such distances. However, it is unlikely that an electron-transfer pathway involving the equivalent tyrosine and cysteine residues is operative for mediating electron transfer from exogenous reduced rubredoxin in 1Fe−SORs. In the crystal structure of *P. furiosus* SOR, tyrosine (Tyr110) is at a subunit interface of the homotetramer and buried in the interior of the protein (*8*). The possibility that the tetrameric quaternary structure is an artifact of crystallization has been considered, but it seems unlikely in light of the extensive subunit interfaces (*8*) and light scattering evidence for tetramers, but not monomers or dimers, in solution.[2]

By analogy with type 1 copper proteins, the alternative electron-transfer pathway in both 1Fe and 2Fe−SORs is via the solvent-exposed δN−histidine Fe ligand in the Y−C−X−X−H sequence (His114 in *P. furiosus* SOR and His118 in *D. desulfuricans* 2Fe−SOR). In type 1 copper proteins, the vibrational modes of the equivalent histidine are selectively enhanced in the resonance Raman spectrum using excitation into the intense (Cys)S(p_π)-to-Cu(d_π) CT transition because the N(p_π) orbital is aligned (imidazole ring makes an angle of 72° to the CuN_2S plane) for overlap with the Cu($d_{x^2-y^2}$) d_π orbital (*19*). In SORs, the imidazole rings of the trans histidines, His114 and His41 in *P. furiosus* SOR and His 118 and His 68 in *D. desulfuricans* 2Fe−SOR, have a propeller twist with each at an angle of ~50° (*P. furiosus* SOR) and ~60° (*D. desulfuricans* 2Fe−SOR) to the FeN_2S plane. Optimal overlap would require the imidazole rings to be orthogonal (90°) (see Figure 8b), but both are positioned for partial overlap of the N(p_π) orbital with the Fe(d_{xy}) orbital, which is the acceptor orbital for the (Cys)S(p_π)-to-Fe(d_π) CT transition (see Figure 8b). This overlap is presumably responsible for the weak enhancement of the symmetric and asymmetric Fe−N(His) stretching modes in *P. furiosus* SOR and *D. desulfuricans* 2Fe−SOR (*6*) in the 190−250 cm^{-1} region, via an *A*-term mechanism. Hence electron transfer via the solvent-exposed histidine residues in 1Fe and 2Fe−SORs will result in increased electron density in Fe(d_{xy}) d_π orbital, thereby facilitating substrate reduction via electron transfer to the superoxide π^* orbital and promoting release of the resultant peroxide (*10*). Further experiments, including mutational studies, will clearly be required to address if one or both of the two potential electron pathways are operational in 2Fe−SORs.

While the above discussion serves to emphasize the close parallels between the electron transfer pathways and resonance Raman enhancement mechanisms in SOR and type 1 copper proteins, the correlation in the resonance Raman spectra is not immediately apparent. The resonance Raman spectra of SOR and type 1 copper proteins using excitation into the equivalent (Cys)S(p_π)-to-Fe(d_π) and (Cys)S(p_π)-to-Cu(d_π) CT bands are very different in the low-frequency region. However, the differences are readily interpretable in terms of the metal−S(Cys) bond lengths. The short Cu−S bond length in type 1 copper proteins (~2.1 Å, *36*) results in a Cu−S(Cys) stretching frequency near 400 cm^{-1}. This leads to strong kinematic coupling and resonance enhancement of cysteinyl deformation modes in the 350−450 cm^{-1} region in type 1 copper proteins (*17*−*21*). The longer Fe−S bond length in oxidized SOR (2.36 Å based on EXAFS measurements, *9*) results in an Fe−S(Cys) stretching frequency near 320 cm^{-1} and optimal kinematic coupling and resonance enhancements for cysteinyl deformation modes in the 270−370 cm^{-1} region. In accord with this interpretation, the resonance Raman spectrum of *P. furiosus* SOR is very similar to that observed for the type 2 Cu center in the

[2] Yeh, A. P., Hu, Y., Jenney, F. E., Adams, M. W. W., and Rees, D. C., unpublished observations.

exogenous histidine-bound form of the His119Gly variant of azurin (*17*, *18*). The type 2 adduct has a CT band at 400 nm, as opposed to 625 nm for the type 1 imidazole-bound adduct of the His119Gly variant. The dramatic change in the energy of the CT band and the resonance Raman spectrum has been attributed to bidentate binding of the exogenous histidines to yield a four-coordinate square planar site with concomitant lengthening of the Cu−S(Cys) bond to ~2.29 Å (*17*, *18*).

The crystallographic data for the oxidized active sites in *P. furiosus* SOR (*8*) and the *D. desulfuricans* 2Fe−SOR (*7*) were ambiguous with respect to the identity or existence of the ligand trans to the cysteine. In two of the four subunits of *P. furiosus* SOR, the conserved glutamate provided the sixth ligand, whereas in the other two subunits of *P. furiosus* SOR and in *D. desulfuricans* 2Fe−SOR, the sixth coordination site is either vacant or occupied by a water molecule. On the basis of X-ray absorption studies of *P. furiosus* SOR, it now seems likely that photoreduction in the X-ray beam is responsible for this discrepancy (*9*). Furthermore, the detailed electronic properties of the oxidized Fe site in *P. furiosus* SOR as deduced by EPR and VHVT MCD spectroscopy (*9*), the number of ligands in the first coordination sphere of the oxidized Fe site in *P. furiosus* SOR as deduced by Fe EXAFS analysis (*9*), and the marked changes in the oxidized absorption spectra that accompany mutation of the conserved glutamate in both 1Fe−SORs (*37* and this work) and 2Fe−SORs (*38*, *39*), are all consistent with a six-coordinate site with glutamate as the ligand trans to cysteine. While the breadth and asymmetry of the predominantly Fe−S(Cys) stretching mode at 323 cm^{-1} suggests some heterogeneity in the high-spin ferric active sites within the homotetramer, the frequency is also best interpreted in terms of a six-coordinate Fe site.

Hemoproteins provide the best frame of reference for comparing the frequencies of axial Fe−S(Cys) stretching modes in five- and six-coordinate sites. The Fe−S(Cys) stretching mode has thus far only been positively identified at 312 cm^{-1} in one six-coordinate heme: the cysteine/histidine axially ligated low-spin ferric heme in cystathionine β-synthase (*40*). As expected, the Fe−S(Cys) stretching frequency increases significantly to ~350 cm^{-1} for the five-coordinate high-spin ferric hemes in cytochrome $P450_{cam}$ (*41*) and chloroperoxidase (*42*). Resonance Raman studies of the cyanide-bound, low-spin adduct of oxidized *P. furiosus* SOR have shown that the Fe−S(Cys) stretching frequency is also relatively insensitive to spin-state changes associated with cyanide binding trans to the cysteinate ligand.[3] Hence, the Fe−S(Cys) stretching frequency in both low-spin and high-spin derivatives of *P. furiosus* SOR is consistent with a six-coordinate site.

The absence of any significant changes in the resonance Raman spectra of wild-type *P. furiosus* SOR on increasing the pH from 7.5 to 10.5 and on mutating the ligating glutamate residue to alanine, coupled with the parallel changes in the UV−visible absorption spectra, suggests that the glutamate ligand is replaced by a common ligand as a result of both the alkaline transition and the E14A mutation. The best candidates for the ligand that replaces the glutamate are hydroxide or lysine 15. The latter suggestion is based on the crystallographic data, which show that the glutamate 14 moves to a position 10.6 Å from the Fe on reduction and that the closest residue to Fe in the reduced active-site structure is lysine 15, which is located 6.6 Å from the Fe. Precedent for an alkaline transition with a similar pK_a involving deprotonation and coordination of a lysine residue adjacent to the ligand coordinating at neutral pH is provided by cytochrome *c* (*43*). Unfortunately, our attempts to discriminate between these two possibilities by detailed resonance Raman studies of samples exchanged into $H_2{}^{18}O$ buffer and globally labeled with ^{15}N have been unsuccessful due to lack of resonance enhancement of the stretching mode of the Fe−ligand bond that is trans to the Fe−S(Cys). While the identity of the ligand remains to be determined, the resonance Raman data demonstrate that the change in ligation induced by the alkaline transition or the E14A mutation has little effect on the strength of the Fe−S(Cys) bond.

Finally, it is appropriate to reevaluate the published resonance Raman results for *D. desulfuricans* 2Fe−SOR (*6*), in light of the more detailed and higher quality data presented herein for *P. furiosus* SOR. The resonance Raman results for *D. desulfuricans* 2Fe−SOR provided the first evidence for cysteinyl ligation of the novel mononuclear Fe center that is now known to constitute the SOR active site (center II). However, prior to the crystallographic data (*7*), it was not possible to discriminate between one or two cysteinyl ligands on the basis of the resonance Raman data (*6*). Moreover, detailed assignments for the SOR center were complicated by resonance enhancement of the rubredoxin-type $Fe(SCys)_4$ center (center I), even with 647 nm excitation. Nevertheless, it is now clear that the majority of the observed bands can be assigned by direct analogy with data presented herein for *P. furiosus* SOR. The only ambiguity comes in the assignment of the bands that predominantly correspond to Fe−S(Cys) stretching and S−C_β−C_α bending modes of the SOR site in 2Fe−SOR. Attempts to remove contributions from center I involved subtraction of the spectrum of the partially reduced sample (center II reduced and center I oxidized), under the assumption that the dominant band in the partially reduced spectrum at 314 cm^{-1} originated exclusively from center I. This assumption no longer appears to be valid, and it now seems likely that center II also has a band at 314 cm^{-1}. However, the relative intensities of the 300 and 314 cm^{-1} bands for the SOR center are inverted compared to the 298 and 323 in *P. furiosus* SOR. As in *P. furiosus* SOR, the Fe−S(Cys) stretching and S−C_β−C_α bending modes are likely to be extensively mixed in *D. desulfuricans* 2Fe−SOR, and investigation of ^{34}S- and ^{54}-Fe-enriched samples will be required to address the contributions of these modes to the 300 and 314 cm^{-1} bands. However, it is clear that the Fe−S(Cys) stretching mode of the SOR active site in *D. desulfuricans* 2Fe−SOR occurs at a significantly lower frequency than that in *P. furiosus* SOR, indicating a longer Fe−S(Cys) bond. Since the Fe−N(His) stretching modes have stronger enhancement in *D. desulfuricans* 2Fe−SOR than that in *P. furiosus* SOR (*6*), this presumably reflects decreased S(p_π)−Fe(d_π) interaction at the expense of the increased histidine N(p_π)−Fe(d_π) interaction. In accord with this interpretation, the histidine imidazole rings that are available for N(p_π)−Fe(d_π) interaction are closer to orthogonality with the FeN_2S plane in *D. desulfu-*

[3] Clay, M. D., Cosper, C. A., Jenney, F. E., Adams, M. W. W., and Johnson, M. K., manuscript in preparation.

ricans 2Fe−SOR (∼60°) than that in *P. furiosus* SOR (∼50°) and hence are expected to have better overlap with the Fe-$(d_{xy})d_{\pi}$ orbital.

SUPPORTING INFORMATION AVAILABLE

Visible absorption spectra of wild-type *P. furiosus* SOR at pH 7.5 and 10.5 and of the E14A variant at pH 7.5; resonance Raman spectra of wild-type *P. furiosus* SOR at pH 7.5 and 10.5 and of the E14A variant at pH 7.5 using 568 nm excitation; resonance Raman spectra of wild-type *P. furiosus* SOR at pH 7.5 in $H_2{}^{16}O$ and $H_2{}^{18}O$ buffer solutions; resonance Raman spectra of wild-type *P. furiosus* SOR at pH 10.5 in $H_2{}^{16}O$ and $H_2{}^{18}O$ buffer solutions; resonance Raman spectra of E14A *P. furiosus* SOR at pH 7.5 in $H_2{}^{16}O$ and $H_2{}^{18}O$ buffer solutions; resonance Raman spectra of natural abundance (NA) and ^{15}N globally labeled wild-type *P. furiosus* SOR at pH 10.5. This material is available free of charge via the Internet at http://pubs.acs.org.

REFERENCES

1. Jenney, F. E., Verhagen, M. F. J. M., Cui, X., and Adams, M. W. W. (1999) *Science 286*, 306−309.
2. Lombard, M., Touati, D., Fontecave, M., and Nivière, V. (2000) *J. Biol. Chem. 275*, 27021−27026.
3. Coulter, E. D. and Kurtz, D. M., Jr. (2001) *Arch. Biochem. Biophys. 394*, 76−86.
4. Chen, L., Sharma, P., LeGall, J., Mariano, A. M., Teixeira, M., and Xavier, A. V. (1994) *Eur. J. Biochem. 226*, 613−618.
5. Moura, I., Tavares, P., Moura, J. J. G., Ravi, N., Huynh, B. H., Liu, M.-Y., and LeGall, J. (1990) *J. Biol. Chem. 265*, 21596−21602.
6. Tavares, P., Ravi, N., Moura, J. J. G., LeGall, J., Huang, Y.-H., Crouse, B. R., Johnson, M. K., Huynh, B. H., and Moura, I. (1994) *J. Biol. Chem. 269*, 10504−10510.
7. Coelho, A. V., Matias, P., Fülõp, V., Thompson, A., Gonzalez, A., and Carrondo, M. A. (1997) *J. Biol. Inorg. Chem. 2*, 680−689.
8. Yeh, A. P., Hu, Y., Jenney, F. E., Adams, M. W. W., and Rees, D. C. (2000) *Biochemistry 39*, 2499−2508.
9. Clay, M. D., Jenney, F. E., Jr., Hagedoorn, P. L., George, G. N., Adams, M. W. W., and Johnson, M. K. (2002) *J. Am. Chem. Soc. 124*, 788−805.
10. Adams, M. W. W., Jenney, F. E., Jr., Clay, M. D., and Johnson, M. K. (2002) *J. Biol. Inorg. Chem. 7*, 647−652.
11. Drozdzewski, P. M. and Johnson, M. K. (1988) *Appl. Spectrosc. 42*, 1575−1577.
12. Shelnutt, J. A., Rousseau, D. L., Dethemers, J. K., and Margoliash, E. (1979) *Proc. Natl. Acad. Sci. U.S.A. 76*, 3865−3871.
13. Czernuszewicz, R. S., LeGall, J., Moura, I., and Spiro, T. G. (1986) *Inorg. Chem. 25*, 696−700.
14. Czernuszewicz, R. S., LaTonya, K. K., Koch, S. A., and Spiro, T. G. (1994) *J. Am. Chem. Soc. 116*, 7134−7141.
15. Loehr, T. M. (1992) *J. Raman. Spectrosc. 23*, 531−537.
16. Spiro, T. G. and Czernuszewicz, R. S. (1995) *Methods Enzymol. 246*, 416−460.
17. Andrew, C. R. and Sanders-Loehr, J. (1996) *Acc. Chem. Res. 29*, 365−372.
18. Andrew, C. R., Han, J., den Blaauwen, T., van Pouderoyen, G., Vijgenboom, E., Canters, G. W., Loehr, T. M., and Sanders-Loehr, J. (1997) *J. Biol. Inorg. Chem. 2*, 98−107.
19. Dong, S. and Spiro, T. G. (1998) *J. Am. Chem. Soc. 120*, 10434−10440.
20. Qiu, D., Kilpatrick, L., Kitajima, N., and Spiro, T. G. (1994) *J. Am. Chem. Soc. 116*, 2585−2590.
21. Qiu, D., Dasgupta, S., Kozlowski, P. M., Goddard, W. A., and Spiro, T. G. (1998) *J. Am. Chem. Soc. 120*, 12791−12797.
22. Czernuszewicz, R. S., Fraczkiewicz, G., Fraczkiewicz, R., Dave, B. C., and Germanas, J. P. (1995) in *Spectroscopy of Biological Molecules* (Merlin, J. C., Ed.) pp 273−276, Kluwer, Dordrecht, The Netherlands.
23. Li, H., Wurrey, C. J., and Thomas, G. J., Jr. (1992) *J. Am. Chem. Soc. 114*, 7463−7469.
24. Fabian, H. and Anzenbacher, P. (1993) *Vib. Spectrosc. 4*, 125−148.
25. Han, S., Czernuszewicz, R. S., and Spiro, T. G. (1989) *J. Am. Chem. Soc. 111*, 3496−3504.
26. Fraga, E., Webb, M. A., and Loppnow, G. R. (1996) *J. Phys. Chem. 100*, 3278−3287.
27. Ungar, L. W., Scherer, N. F., and Voth, G. A. (1997) *Biophys. J. 72*, 5−17.
28. Newton, M. D. (1991) *Chem. Rev. 91*, 767−792.
29. Farver, O. and Pecht, I. (1981) *Proc. Natl. Acad. Sci. U.S.A. 78*, 4190−4193.
30. He, S., Modi, S., Bendall, D. S., and Gray, J. C. (1991) *EMBO J. 10*, 4011−4016.
31. Sigfridsson, K., Young, S., and Hansson, Ö. (1996) *Biochemistry 35*, 1249−1257.
32. Qin, L., and Kostic, N. M. (1996) *Biochemistry 35*, 3379−3386.
33. Ascenso, C., Rusnak, F. M., Cabrito, I., Lima, M. J., Naylor, S., Moura, I., and Moura, J. J. G. (2000) *J. Biol. Inorg. Chem. 5*, 720−729.
34. Lombard, M., Fontecave, M., Touati, D., and Nivière, V. (2000) *J. Biol. Chem. 275*, 115−121.
35. Page, C. C., Moser, C. C., Chen, X., and Dutton, P. L. (1999) *Nature 402*, 47−52.
36. Guss, J. M., Bartunk, H. D., and Freeman, H. C. (1992) *Acta Crystallogr., Sect. B 48*, 790−811.
37. Abreu, I. A., Saraiva, L. M., Soares, C. M., Teixeira, M., and Cabelli, D. E. (2001) *J. Biol. Chem. 276*, 38995−39001.
38. Coulter, E. D., Emerson, J. P., Kurtz, D. M., Jr., and Cabelli, D. E. (2000) *J. Am. Chem. Soc. 122*, 11555−11556.
39. Lombard, M., Houée-Levin, C., Touati, D., Fontecave, M., and Nivière, V. (2001) *Biochemistry 40*, 5032−5040.
40. Green, E. L., Taoka, S., Banerjee, R., and Loehr, T. M. (2001) *Biochemistry 40*, 459−463.
41. Champion, P. M., Stallard, B. R., Wagner, G. C., and Gunsalus, R. P. (1982) *J. Am. Chem. Soc. 104*, 5469−5472.
42. Bangcharoenpaurpong, O., Hall, K. S., Hager, L. P., and Champion, P. M. (1986) *Biochemistry 25*, 2374−2378.
43. Ferrer, J. C., Guillemette, J. G., Bogumil, R., Inglis, S. C., Smith, M., and Mauk, A. G. (1993) *J. Am. Chem. Soc. 115*, 7507−7508.

BI025833B